Journal of Basic and Environmental Sciences, 7 (2020) 140-153

ISSN
Online: 2356-638
Print: 2536-9202

Research paper Open Access

Synthesis and Characterization of Functionalized activated Carbon for Removal of Uranium and Iron from Phosphoric Acid

A. A. Abdel-Samad, M. M. Abdel Aal, E. A. Haggag, W. M. Youssef
Nuclear Materials Authority, P.No. 530 El- Kattamia, El- Maadi, Cairo, Egypt

Abstract

Uranium and iron sorption from synthetic phosphoric acid was carried out onto activated pistachio nut. This activated carbon was modified by adding some functional groups which have great ability to attract uranium from its solution. The different factors affecting uranium and iron adsorption have been investigated. The obtained results clear that, the sorption preferred conditions were; solution pH of 3, shaking time of 60 min., room temperature, and adsorbent amount is 1g/L. Based on kinetic modeling investigation, the sorption process of uranium and iron is following to pseudo-second order mechanism. From the results, the uranium and iron sorption from synthetic phosphoric acid, with only about 3% loss of P_2O_5, onto activated pistachio nut was found to occur through physical sorption process. The adsorption process has been found to agree with the Langmuir isotherm and confirms with the concept of the matrix diffusion controls according to Homogeneous Particle Diffusion Model (HPDM).

Keywords Uranium, Iron, Sorption, Phosphoric Acid, Activated Pistachio Nut.
Received; 13 Jun 2019, Revised form; 12 Dec. 2019, Accepted; 12 Dec. 2019, Available online 1 April 2020.

1. Introduction

Phosphoric acid has many applications. Due to its non-toxic and mildly acidic nature, it is used in food flavoring, beverages, dental products, cosmetics, and skin care products [1]. Industrially, it is used mainly in the production of phosphate fertilizers [2]. It is also widely used as an electrolyte, etching agent, rust removal agent, pH modifier, household cleaning agent, dispersing agent, sanitizing agent, produce materials such as detergents, water treatment chemicals, leavening agents and animal feed supplements [3]. Phosphoric acid is however mainly used in the fertilizer field where it serves as an intermediate between phosphate ore and major end products such as ammonium phosphate, triple superphosphates, liquid mixed fertilizers, high-analysis solid mixed fertilizers and some types of nitric phosphates [4]. Phosphorites actually considered as an important alternate or secondary source for uranium [5]. Uranium content of phosphate rock varies from 20 ppm to 500 ppm. The majority (80-90%) of uranium content in phosphate rock transfers to the final fertilizer product during mineral processing and is thus dispersed on agricultural soils, leading to the contamination of topsoils as well as ground- and surface waters [6].

Orabi et al. using prepared amine-impregnated cellulose as adsorbent for uranium originated from El-Sebaiya phosphate ore. The impregenation process was carried out by copolymerization between pretreated cellulose and a mixture of (tri-ethyl amine and epi-chorohydrine). The obtained equilibrium data were found to be satisfactory fitted with Langmuir isotherm. A maximum-metal uptake of 56.5 mg U/g AIC was observed at the obtained optimum conditions [7]. Hussein et al. develop the ceramic adsorbent media in order to remove uranium from crude phosphoric acid. The adsorption capacity of the studied commercial ceramic sample was determined (about 11 mg U/g ceramic), the equilibrium adsorption isotherms for uranium adsorption on the studied ceramic sample were determined [8].

Iron is one of the most important impurities, the content of iron as (Fe_2O_3) in fertilizer grade phosphoric acid (50% P_2O_5) must be not more than 1.5% Fe_2O_3 [9]. The Egyptian phosphate ores when leached with H_2SO_4 or recycled H_3PO_4, the produced phosphoric acid (50% P_2O_5) contains 4 or 2.7% Fe_2O_3, respectively [10]. While higher iron content negatively affects the solubility of fertilizer P_2O_5 in water [11].

Removal of heavy metals from phosphoric acid and phosphates is environmentally important referring mainly to their toxicity [12]. Purification of acid is necessary for its use in foodstuffs, in animal feed additives, detergents, food products, toothpaste and fertilizers [13, 14]. Removal of heavy ions from phosphoric acid has been studied using many techniques [15-19].

Abdallah et al. using polyvinyl alcohol and zirconium oxide composite as adsorbent to removal iron metal through batch experiment. The optimum time is 60 min. and the achieved results imply that the removal percentages of 25 mg/L Fe^{+3} from 1 to 70% phosphoric acid are in the range of 85.7 and 45.6%, respectively. The experimental results were found to fit with Langmuir isotherm model [10]. Sultanbayeva et al. [20] used zeolite to remove of Fe^{2+} and Al^{3+} from phosphoric acid. They found that, the highest degrees of acid purification were achieved in the first 5 min. of the process with the removal of 60.2% for Fe^{+2}, 95.4% for Al^{+3}. On the other hand, El-Zahhar et al. [21] prepared polyacrylamide grafted activated carbon (PA-AC) from chemically activated carbon of rice husk and rice straw to remove iron from wet-phosphoric acid solution. They claimed that experimental results were found to fit with

Langmuir isotherm model with maximum sorption capacity 6.15 mg/g.

Different techniques were studied for purification of phosphoric acid as; precipitation, ion exchange, solvent extraction [22-28], precipitation [29-31], adsorption [32-35], ion exchange and reverse osmosis were also used [36,37].

Various modified natural materials like olive bagasse, potato peel, soybean straw, nut shells and lots of other agricultural wastes have been applied to produce activated carbon [38-41].

In the present work Pistachio nuts shell (PNS) was used to prepare functionalized activated carbon as adsorbent material. The prepared adsorbent was characterized and used for uranium and iron adsorption from phosphoric acid solutions. The parameters affecting the sorption process were studied and optimized.

2. Experimental

2.1. Chemicals and Reagents

All chemicals used in this study were of analytical grade reagent and were used without further purification. Ferrous sulphate, uranyl sulphate, Ethylene diamine tetraacetic acid and bromine were supplied from Aldrich. Ammonium meta-vanadate and potassium bromide (GFS chemicals, USA) and each of methyl orange, phenolphthalein, ortho phosphoric acid, and nitric acid were purchased from Merck. Phosphoric acid, hydrochloric acid, acetic acid, and sodium hydroxide solutions (Adwic), the last two solutions were used to adjust the pH of the aqueous solutions.

2.2. Preparation

The preparation processes involved objected synthetic phosphoric acid solution and activated pistachio nut.

2.2.1. Preparation of synthetic phosphoric acid

Synthetic uranium and iron - bearing phosphoric acid solution was prepared. The prepared phosphoric acid solution contained 44% P_2O_5 has thus been prepared from Adwic 85% P_2O_5 phosphoric acid by proper dilution. A known amount of uranyl sulfate and iron sulfate were dissolved in the prepared synthetic phosphoric acid solution to attain an assay of 150 ppm uranium and 2.5% ferric oxide.

2.2.2. Preparation of activated pistachio nutshell

Pistachio nuts shell (PNS) was collected from the local markets of Cairo (Egypt). It was washed with hot distilled water to remove any adherent impurities, dried at 105 °C for 24 hours in vacuum dryer, ground and then sieved to 1-2 mm. PNS soaking with acetic acid at room temperature with weight ratio 1:3 (PNS: CH_3COOH), the PNS and acetic acid solution were mixing for 3 days with occasional stirring. The treated shell dried at 105°C in the vacuum oven dryer. The treated sample was activated by the continuous nitrogen flow (100 ml/min at STP) in a programmable electrical horizontal tubular furnace (Nabertherm, Labothem Model R50/250/12) using a quartz tube (450 mm × 40 mm), the activation temperature was increased at a rate of 10 °C/min from room temperature to 600 °C and held for 2 hours. The carbonized sample was cooled to room temperature under N_2 flow, then grounded and sieved. After that, the sample washed several times with deionized water and dried at 110 °C. The obtained sample is designated as the activated pistachio nuts shell, APNS.

2.3. APNS Characterizations

The textural properties of prepared activated carbons were determined from the N_2 adsorption-desorption isotherms at -196 °C using NOVA2000 gas sorption analyzer (Quantachrome Corporation) system. Prior to measurement, the samples were degassed under vacuum at 150 °C and 10^{-5} Torr overnight to ensure a dry clean surface. The adsorption isotherm was constructed as the volume adsorbed (V cm^3/g) versus the equilibrium relative pressure P/P°.

A thermogravimetric analysis (TGA) was performed for prepared activated carbon (APNS) with thermo-analyzer ([D-50] Shimadzu, Japan) at a nitrogen flow rate of 20 mL/min and a heating rate 10 °C/min up to 1000 °C.

The surface morphology and topographic analysis of the adsorbent samples were examined by Scanning electron microscopy (SEM) JSM-5500 (JEOL Ltd., Japan) instrument with a 30 kV accelerating voltage, which was dried overnight at approximately 105 °C under vacuum, then covered with a thin layer of gold for charge dispersal.

High-resolution transmission electron microscopy (HRTEM) and energy dispersive X-ray (EDS) spectroscopy (JEOL 2100F TEM) was utilized to get high magnification micrographs of the prepared samples. The instrument was operated at an accelerating voltage of 200 kV. The samples were subjected to ultrasonic in ethanol for 30 min and then dropped on a carbon-coated Cu TEM grid.

Fourier transform infrared spectroscopies (FT-IR) were conducted using a Perkin-Elmer 1720 spectrometer in the range 400 and 4000cm^{-1}. The samples were mixed with KBr (1:500 ratios) then pressed under vacuum.

Supernatant pH was determined using a Jenway pH-meter (model 3510, UK). 0.2 g of the adsorbent in 25 mL of pre-boiled distilled water was shaking for 48 h; then filtered and the pH of the supernatant was measured. And the pH_{pzc} of the prepared samples was measured according to (A.F. Hassan *et al.*, 2013).

Bulk contents of C, H, S and N in the samples were analyzed by 2400 Series II CHNS/O elemental analyzer (Perkin Elmer).

2.4. Sorption Experiments

The removal of uranium and iron from phosphoric acid solution was studied using APNS, where a constant volume of the acid solution was mixed with the appropriate amount of adsorbent and left with stirring to suitable time. After stirring the acid solution was separated from the adsorbent and the concentration of uranium, iron, and P_2O_5 were measured. The removal percentage was calculated as:

$$R\% = \frac{C_o - C_e}{C_o} \times 100 \quad \text{..... (1)}$$

Where Co and Ce are the initial and equilibrium of uranium, iron, and P_2O_5 concentrations in solution (mg/L), respectively. The amount of adsorption qe (mg/g) was calculated from the difference of concentrations in the aqueous solution at the equilibrium time according to relation (2):

$$q_e = (C_o - C_e) \times \frac{V}{m} \quad \ldots\ldots\ldots\ldots (2)$$

Where V is the volume of solution (L), m is the weight of the adsorbent (g). The distribution coefficient (Kd) of uranium, iron, and P_2O_5 between the aqueous bulk phase and the solid phase was calculated from the following relation (3):

$$K_d = \frac{C_o - C_e}{C_e} \times \frac{V}{m} \quad \ldots\ldots\ldots\ldots\ldots (3)$$

2.5. Elution Experiments

The metal ion concentrations adsorbed onto the APNS, can be determined as the difference between the initial and equilibrium concentrations of the metals in the aqueous phase. After elution the concentration of the metal was determined in the aqueous phase after elution to determine the elution percent for the studied metal by relation (4).

$$\text{Elution \%} = \frac{Ce}{C_o - Ce} \times 100 \quad (4)$$

Where C_o and Ce are the initial and equilibrium metals concentrations in the aqueous phase before and after sorption process, respectively, and Ce gives the concentrations of the removal metals in the aqueous phase after elution.

2.6. Batch investigation

The sorption of uranium (VI) and iron from synthetic phosphoric acid has been studied by using APNS. The effect of contact time, pH, initial concentration of uranium and iron, dose adsorbent concentration, stirring speed, and temperature on the uranium and iron sorption efficiency have been investigated, with concentrated on P_2O_5 loss percent. Unless otherwise stated, all experiments were carried out by contacting a fixed weight of 0.01 g adsorbent with a fixed volume of 10 ml from the synthetic phosphoric acid solution (44% P_2O_5 with 150 mg U/L and 2.5 % iron) under the at room temperature (25˚C) for one hour stirring time and 390 rpm as stirring of speed.

3. Results and Discussion

3.1. Surface area and pore structure

Surface area and pore structure of the prepared APNS sample calculated from N_2 adsorption/desorption technique are illustrated in Figure (1) and summarized in Table (1).

The adsorption isotherms of the adsorbent were the mixture of type I and IV according to IUPAC classification [17] at low relative pressures the sharp increase in volume indicated adsorption in micro pores as in type I isotherm. While type IV with H_4 hysteresis loop was appeared at intermediate and high relative pressures, indicated monolayer–multilayer adsorption followed by capillary condensation in narrow slit-like pores. As shown in Figure (1) the area of the hysteresis loop increased with carboxilic impregnation. These indicate that the APNS sample has a mixture from the microporous and mesoporous adsorbent.

The specific surface area S_{BET} (m^2/g) was calculated from the linear plot of the BET equation, micropore surface area S_μ(m^2/g) and micropore volume V_μ (cc/g) were calculated using t-plot method. The total pore volume V_T(cc/g) corresponding to the volume of N_2 near to saturation at p/p° ≈ 0.95. The average pore radius (r^-, nm) could be calculated according to the following equation:

$$r^-(\text{nm}) = \frac{2V_T(\text{ml/g})}{S_{BET}(\text{m}^2/\text{g})} 10^3 \quad (5)$$

Upon analysis of data in Table (1) (i) the S_{BET} and S_μ for APNS sample were 1668.3 m^2/g and 1195.9 m^2/g, where the micropore surface area represented 71.7 % from the total surface area. Also, the V_T and V_μ were 2.375 cc/g and 0.6622 cc/g. Moreover, the V_μ is 27.9 % from the total pore volume. (ii) The average pore radius of the APNS sample is 2.85 nm. (iii) The activation of pistachio nutshell with acetic acid creates the high surface area, where, H_3PO_4 has two important functions: it promotes the pyrolytic decomposition of the initial material and promotes the formation of the cross-linked structure. Moreover, H_3PO_4 allows the development of both micropores and mesopores in the activated carbon **[18]**.

Table (1): Textural parameters of APNS sample

Sample	S_{BET} (m^2/g)	S_μ (m^2/g)	S_{EX} (m^2/g)	S_μ/S_{BET} (%)	V_T (cc/g)	V_μ (cc/g)	V_μ/V_T (%)	r^-(nm)
APNS	1668.3	1195.9	472.4	71.7	2.375	0.6622	27.9	2.85

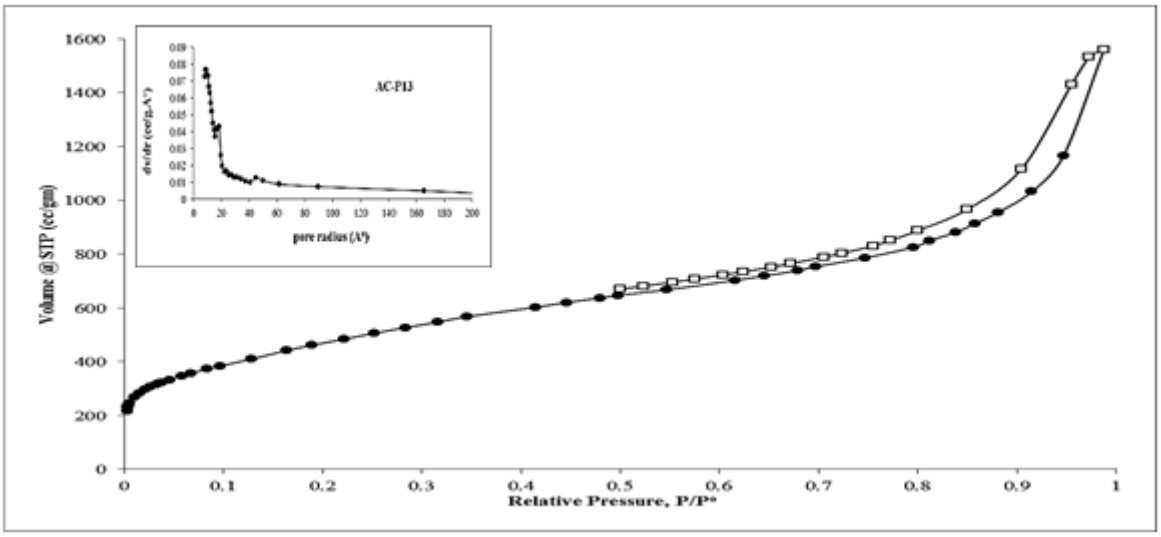

Fig. (1): N2-adsorption/desorption isotherms and pore size distribution for the APNS sample

3.2. SEM and HR-TEM

SEM images of the APNS activated carbon sample are shown in Fig. (2) a, b. SEM images illustrated irregular structure with cracks and crevices on the surface of the activated carbon and some grains in various sizes in large holes. This confirmed amorphous and heterogeneous structures. The chemical activation process was found effective in creating a large surface area with well-developed pores with different sizes shapes on the surface of pistachio nut activated carbon. Moreover, these pores are considered as channels to the microporous network.

TEM images for APNS are shown in Fig. (2) c-f. It is observed that the structure of the prepared activated carbon was consisting from pores structure with different sizes mainly in micropore level, which also interconnected with each other to form the internal microporous network. The porous structure was formed by the disordered packing of carbon sheets (graphitic layers with randomly arranged) and clusters. TEM images were clearly confirming the nature of the amorphous structure [19].

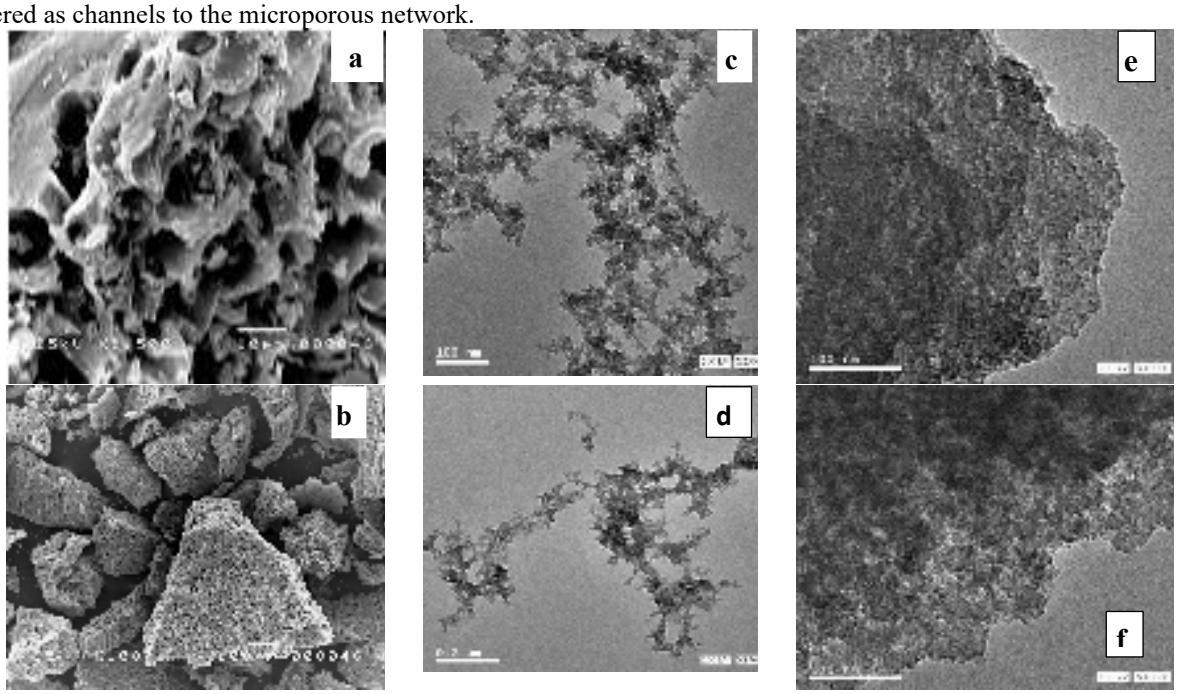

Fig (2): (a) and (b) SEM image of APNS sample, (c) - (f) TEM image for APNS sample

3.3. Thermal analysis

The thermal decomposition behavior of the biomass (related to the chemical composition and chemical bonding in the material structure) is essentially determining the shape of the TGA profile. TGA profile of the pistachio nut and APNS samples show in Figure (3). The TGA profile of the pistachio nutshell shows 10.2 wt% weight loss at 150 °C corresponds to the removal of physically adsorbed water. The weight loss between 250 and 400 °C may be attributed to the decomposition of cellulose and hemicellulose and removal of condensable gasses (methanol, acetic acid, and wood tar) and incondensable gasses (H_2, CH_4, CO, CO_2, H_2O). And the weight loss in the

range 420-700 °C can be assigned to lignins decomposition. There is no change in weight loss over than 750 °C. where the lignocellulosic structure was completely decomposition. On the other hand, the TGA profile of APNS sample show 13.5 % weight loss at about 150°C related to desorption of adsorbed moisture, the great physically adsorbed water over APNS than in raw material is due to the high surface area APNS sample and the presence of hydrophilic C-O functional groups [20, 21]. Then, there is no change in TGA profile up to 750 °C.

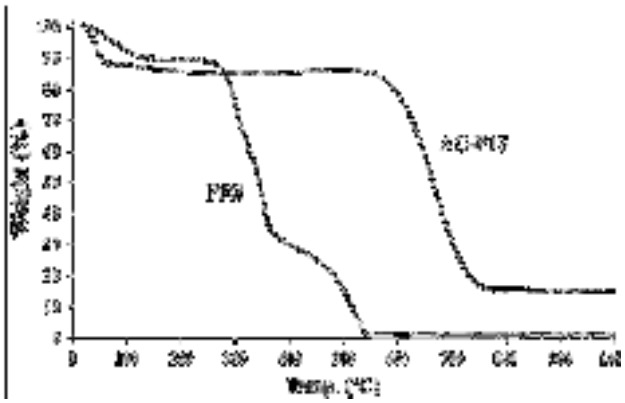

Fig (3): TGA for Pistachio nutshell (PNS) and APNS sample

3.4. Surface chemistry

The surface chemistry of carbon materials is determined by the acidity and basicity of their surface. Table (2) shows the values of pH for adsorbents and the values of pH_{pzc}. The pH of APNS sample is 3.12, this indicates that this the acidic functional groups are predominating largely on this carbon surface. One of the most important characteristics of carbon adsorbents is pHpzc, which indicates the point in which the adsorbent surface charge density is zero. When the pH value of the solution is less than pHpzc the adsorbent reacts as a positively charged surface and when it is greater than pHpzc the adsorbent functions as a negatively charged surface [1]. The amount of pHpzc obtained in this research was 2.98, This low pH_{PZC} value also showed the dominance of acidic groups on the surface of the activated carbons. The pH_{PZC} value indicates that carbon produced from phosphoric acid activation is acidic and classified as L–Carbon [22].

The chemical composition of the precursor (pistachio nut shells), acetic acid–activated carbons is given in the Table (3). For APNS sample, it is clear that prepared APNS has higher contents of carbon and lower contents of oxygen, hydrogen and nitrogen compared to the raw material (PNS) this resulted due to acetic acid activation has the dehydration effect and polymeric deformation. Also, the acetic acid activation led to decrease H/C ratio from 0.14 in PNS sample to 0.03 [23,24]. Moreover, The O/C ratio decreased from 0.97 in PNS sample to 0.25 in the OP13 sample [25].

Table (2): Physical and chemical properties of PNS and APNS samples

Sample	Bulk Density g/mL	Moisture content (%)	Ash content	pH	pH_{PZC} or pH_{IEP}
PNS	0.689	2.4	1.08	6.57	6.46
APNS	0.307	9.6	4.95	3.12	2.98

Table (3): Chemical composition of PNS and APNS samples

Sample	C %	H %	N %	S %	O % (by difference)	H/C	O/C
PNS	47.3	6.41	0.2	0.24	45.85	0.14	0.97
APNS	78.21	2.0	0.43	0.01	19.4	0.03	0.25

Figure (4) illustrate the FTIR spectrum APNS sample before and after U(VI) and iron adsorption. For all spectra coming from the oxygenated group, The spectra of activated carbon before adsorption found that the broadband located around 3415 cm^{-1} can be assigned to the –OH stretching vibration mode of hydroxyl functional groups [26,27]. The two strong peaks located at 2853 and 2923 cm^{-1} related to C–H stretching vibration for $–CH_2–$ and $–CH_3$. The bands at 1745 and 1716 cm^{-1} corresponding to C=O stretching vibration in the carboxylic group, lactones, and anhydride. The broadband located at 1600 cm^{-1} attributed to C=C stretching vibration in aromatic ring of quinone and Keto–enol group [28]. The bands at 1450, 1438, 1400 and 1385 cm^{-1} assigned to C–O stretching in carboxylate groups. Also, The stretching vibrations of $–CH_3$ at 1385 cm^{-1} are related to methyl structures [29]. The broadband around 1300 and 900 cm^{-1} with maxima at 1100 and 1046 cm^{-1} found with oxidized carbons and have been assigned to C–O stretching in acids, alcohols, phenols, ethers and/or esters groups [30]. Nevertheless, it is also a characteristic of phosphorous and phosphor carbonaceous compounds present in the phosphoric acid activated carbons [31]. Assignment in this region is difficult because absorption bands are overlapped. The peak at 1190–1200 cm^{-1} may be also assigned to the stretching mode of hydrogen–bonded P–O, to O–C stretching vibrations in P–O–C (aromatic) linkage and to POOH [32]. The shoulder at 1100 cm^{-1} was ascribed to ionized linkage $P^+–O^-$ in acid phosphate esters and symmetrical vibration in a P–O–P chain [33]. The bands at 875 and 793 cm^{-1} are due to out of plane deformation mode of C–H for different substituted benzene rings. Finally, 600 cm^{-1} we observed a most intense peak corresponding to the presence of hydroxyl O–H stretching vibrations.

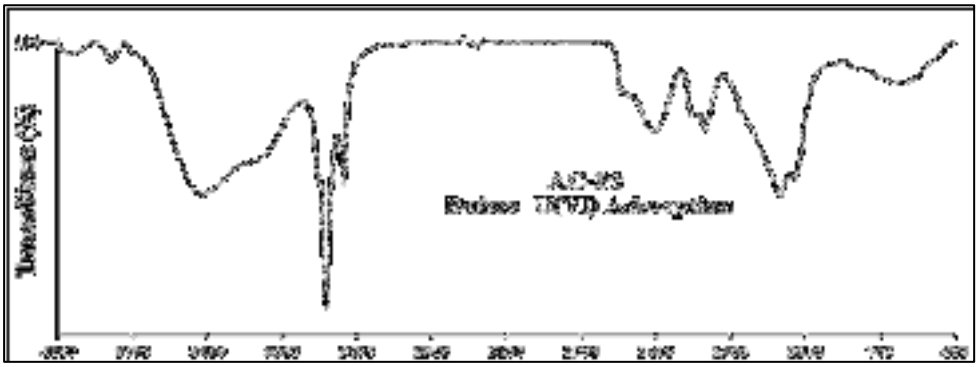

Fig (4): FTIR spectra of APNS sample

Surface acidity and basicity is a crucial factor for describing the chemistry of carbon adsorbent surface. In the current research, the acidity and basicity of APNS were calculated to be 1.831 meq/g and 0.081 meq/g respectively. Results prove the acidity nature of APNS surface which is due to the presence of oxygen containing groups like carboxylic, anhydrides, lactones, phenols, while basicity could be a result of the presence of oxygen-free lewis sites, carbonyls, pyrone and chromene [33]. Observing a higher level of surface acidity than basicity for carbon adsorbent surface is in agreement with results concluded from pH_{pzc} value. Also, the phosphoric acid activation lead to creates a new carboxylic group [34], which will enhance its sorption toward removal of the metallic cation (such as uranium cation) from aqueous solution [35].

3.5. Uranium Sorption

3.1.1. Effect of Contact Time

The required contact time for sorption to be completed is important to give insight into the kinetics of the sorption process a range from 5 to 120 minutes was studied as a contact time under fixed conditions of 0.01 g resin, 10 ml aqueous solution assaying 150 mg U/L and pH of 2 at room temperature. Also, it gives information on the minimum time required for considerable adsorption to occur, and also time for equilibrium could give information about the movement of uranium and ferric ions from the bulk synthetic solution toward the adsorbent surface at pH value of 2.5. Fig. (5) shows when the contact time increases from 5 to 120 minutes, the percent of adsorption increases until it remained constant (42% for uranium and 12% for iron) at about 60 minutes with 2.5% loss of P_2O_5., which was then taken as the equilibrium time.

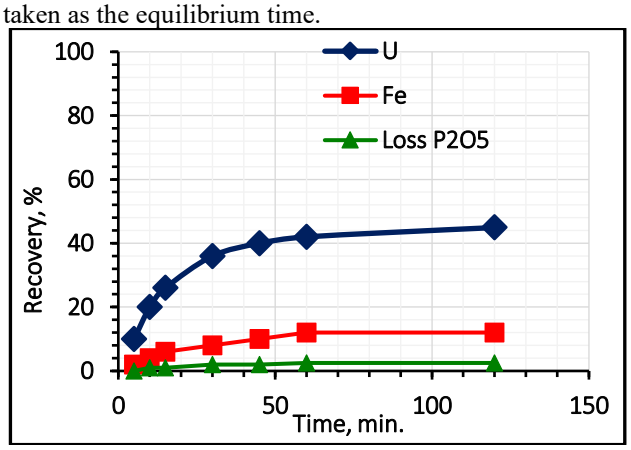

Fig (5): Effect of contact time on sorption of uranium and iron

3.1.2. Effect of pH

The pH of the aqueous solution is an important variable in the adsorption operation. Therefore, the effect of pH upon adsorption of uranium and iron by APNS was studied in the pH range of 0.5 to 4.0 using fixed conditions of 0.01 g resin, 10 ml aqueous solution assaying 150 mg U/L and 1 h contact time at room temperature. From the obtained results plotted in Figure (6), one could observe that uranium and iron adsorption efficiency increased with increasing pH values. The highly adsorption efficiency obtained at pH value of 3(50% for uranium and 16% for iron), with slightly loss of P_2O_5. After this pH value slightly decrease of adsorption efficiency would be found. Thus, the preferable pH value considered 3.

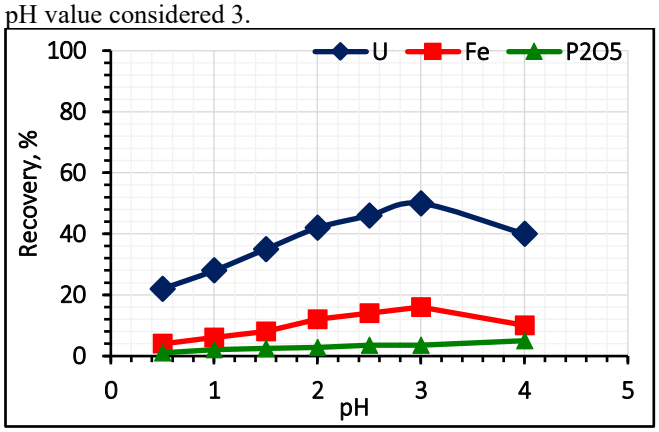

Fig (6): Effect of pH on sorption of uranium and iron

3.1.3. Effect of Initial Uranium Concentration

The effect of initial uranium concentration on the adsorption efficiency of the APNS was studied. A series of experiments were performed by contacting a fixed weight of 0.01 g APNS against 10ml synthetic phosphoric acid with different concentration of uranium ranged from 50 up to 600 mg/L under fixed conditions of 0.01 g APNS, 10 ml aqueous solution assaying 2.5 % iron, 60 minutes contact time and pH of 3 at room temperature. The adsorption capacity was shown in Fig. (7), uranium and iron adsorption efficiency decreased with increasing uranium initial concentration because the uranium amount increase with the same mass of APNS. Therefore, it can be ascertained that the maximum loading capacity of uranium upon APNS is 100mg/g equivalent to 100 g/Kg APNS.

3.1.4. Effect of Dose adsorbent Concentration

Different weights of the adsorbent were used for adsorption of uranium and iron at pH value of 3 and 60 minutes as contact time within dose range of 0.01 g to 0.3 g

in 10 ml of synthetic phosphoric acid while the other parameters were kept constant. The results in Figure (8) show that a significant increase in the adsorption of uranium and iron ions was observed with increasing the adsorbent dose. From the obtained data it noticed that the U uptake (mg/g) was sharply enhanced by increasing the U concentration from 50 to 600 mg/L. Therefore, it can be ascertained that the maximum loading capacity of U upon APNS is 100 mg/g.

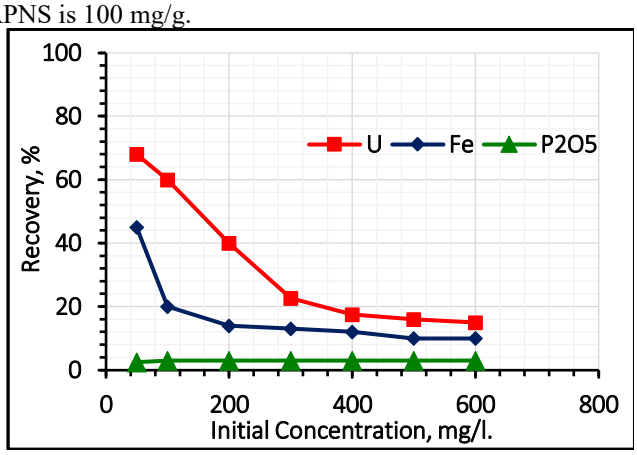

Fig (7): Effect of initial uranium concentration on sorption of uranium and iron

The greater availability of exchangeable sites for the ions, i.e. more active sites is available for binding of uranium and iron ions.

Further increase in adsorbent dose was produced insignificant increase in adsorption. This finding could be explained as a result of cluster formation by adsorbent particles resulting in decrease of surface area and surface-active sites on the adsorbent [42,43].

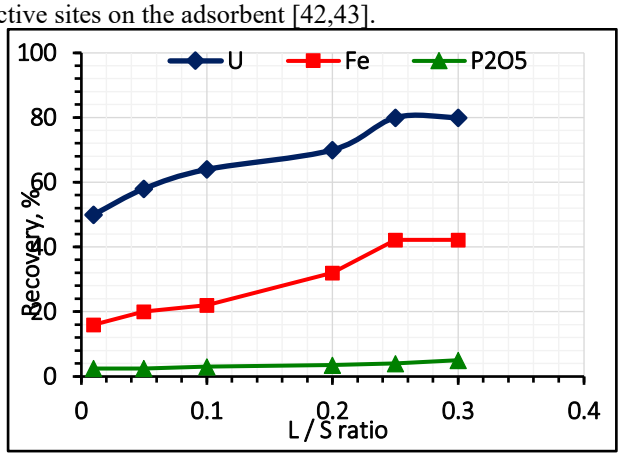

Fig (8): Effect of dose adsorbent concentration on sorption of uranium and iron

3.1.5. Effect of Initial Iron Concentration

The effect of initial iron concentration on the adsorption efficiency of the APNS was studied. A series of experiments were performed by contacting a fixed weight of 0.01 g APNS against 10ml synthetic phosphoric acid with different concentration of iron ranged from 0.5 to 6.0 %. The adsorption capacity was shown in Fig. (9), uranium and iron adsorption efficiency decreased with increasing iron initial concentration because the iron amount increase with the same mass of APNS. From the obtained data in Figure (9), it noticed that the iron uptake (mg/g) was sharply enhanced by increasing the iron concentration from 0.5 to 6 %. Therefore, it can be ascertained that the maximum loading capacity of iron upon APNS is 3333 mg/g.

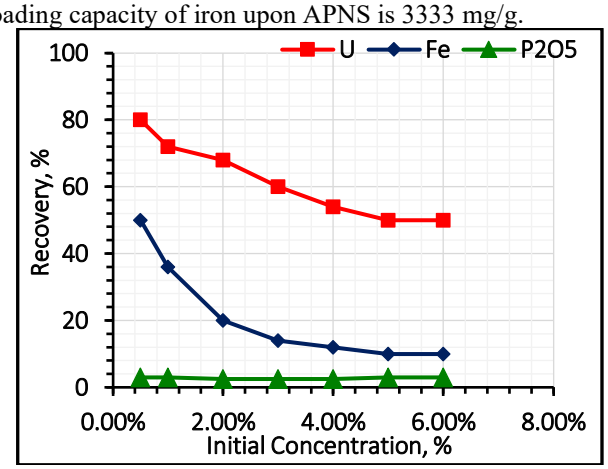

Fig (9): Effect of initial iron concentration on sorption of uranium and iron

3.1.6. Effect of Stirring Speed

Agitation is an important parameter in adsorption phenomena, influencing the distribution of the clay in the bulk solution and the formation of the external boundary film [44]. In this respect, mechanical stirring speed effect on uranium and iron sorption process was studied for the different stirring speed range from 100 to 500 rpm. however; the other parameters were fixed at APNS amount of addition, 0.01 g, 10 ml synthetic phosphoric acid (uranium 150 ppm iron 2.5% P_2O_5 44%) with pH 3, Stirring time of 60 min and room temperature. The experimental result was given in Fig. (10) A relation between adsorption efficiency and mechanical stirring speed show that, as the stirring speed increased from 100 to 500 rpm, the uranium and iron adsorption efficiency increase with slightly decrease of P_2O_5 until 400 rpm. Generally, high agitation speed causes a decrease in the boundary layer and so decreases the resistance of transportation. Finally, this enhances the transfer rate to the surface of the adsorbent, which is called diffusion-controlled mechanism [45].

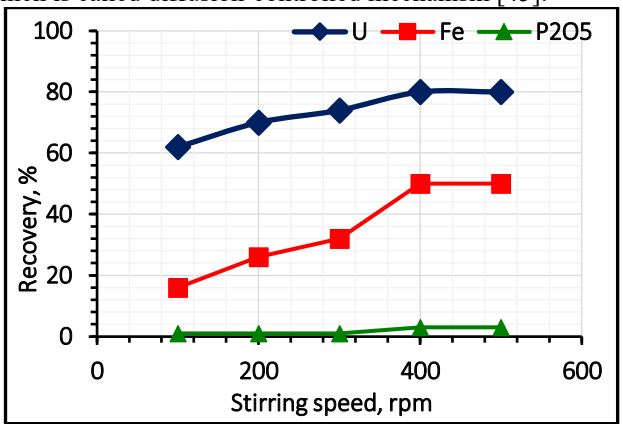

Fig (10): Effect of stirring speed on sorption of uranium and iron

3.1.7. Effect of Temperature

To study the effect of temperature on uranium and iron adsorption efficiency, a series of the adsorption experiments were performed using different temperatures ranging from 25 °C up to 60 °C at the fixed conditions of 0.01g APNS / 10 ml synthetic phosphoric acid with pH 3.

The obtained result was shown in Fig. (11), revealed that uranium adsorption efficiency decreased with increasing temperature. This indicates that the reaction is an exothermic process.

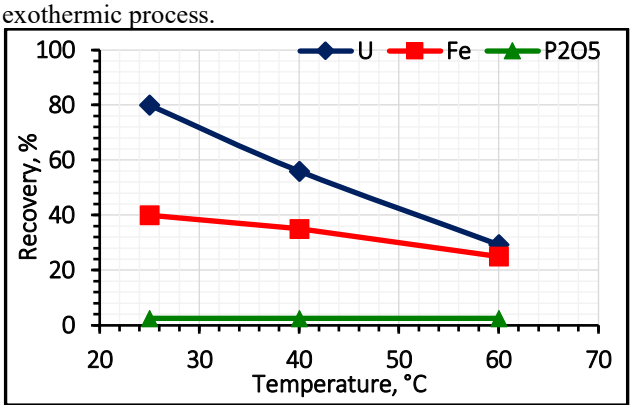

Fig (11): Effect of temperature on sorption of uranium and iron

3.2. Adsorption Kinetics and Mechanism of Uranium

The data obtained from batch experiments which were performed at different temperatures (25–60) ^{0}C were evaluated by using the simple Lagergren equation [46] to determine the adsorption rate of uranium interactions assuming pseudo first order kinetics:

$$\log(q_e - q_t) = \log q_e - \left(\frac{k_1}{2.303}\right)t \qquad (5)$$

where q_t and q_e are the amounts of uranium adsorbed (mg/g) at time, t (min) and equilibrium time (60 min), respectively and K_1 is the pseudo first order Lagergren adsorption rate constant (min $^{-1}$). The K_l values could be obtained by plotting log ($q_e - q_t$) versus t for adsorption of uranium at different temperatures as shown in Fig. (12). The values of the first order rate constant (K_{lU}) and correlation coefficient (R^2) obtained from these plots are listed in Table (4). The values of K_{lU} indicate that the rate of the process decreases with temperature.

The first order mechanism suffered from inadequacies when applied to uranium sorption on the APNS. One of the major discrepancies was observed when q_e values obtained from the pseudo first order plots were compared with the experimental q_e values are seen in Table (4). The experimental q_e values differed from the corresponding theoretical values. Thus, the interaction of uranium with the APNS does not follow the first order kinetics.

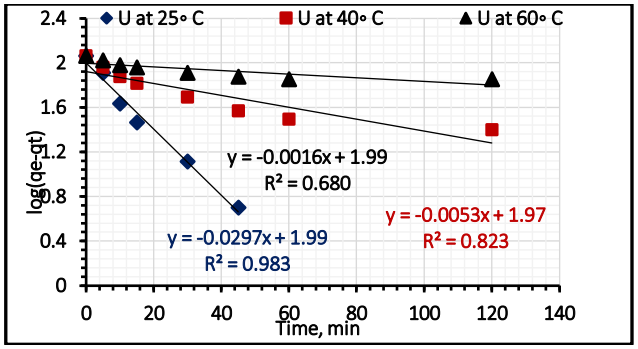

Fig (12): Lagergren plots for the adsorption of uranium

In order to ensure the description of the kinetics, second order kinetic equation was applied. The pseudo second order kinetics can be represented by the following linear equation [47]:

$$\frac{t}{q_t} = \frac{1}{K_2 q_e^2} + \left(\frac{1}{q_e}\right)t \qquad (6)$$

where K_{2U} is the second order rate constant (g.mg^{-1}min^{-1}). The kinetic plots of t/q_t versus t for uranium are shown in Figure (13).

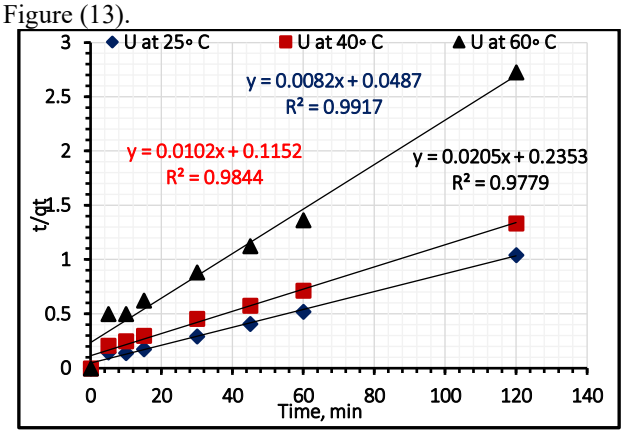

Fig (13): Pseudo second-order plots for the adsorption of uranium

The plots show straight lines with good linearity temperatures. The calculated correlation coefficients are closer to unity for the pseudo second order kinetic model. The calculated equilibrium adsorption capacity (q_e) is consistent with the experimental data. The K_{2U} values show the applicability of the above equation for the resin. Therefore, the sorption reaction can be approximated more favorably by the pseudo second order sorption as the predominant mechanism.

Table (4): Data of kinetic parameters for uranium adsorption onto APNS

Temp, °C	Lagergreen pseudo first-order				pseudo second order			
	K_1 (min $^{-1}$)	q_{ecal} (mg/ g)	q_{eexp} (mg/ g)	R^2	K_2 (min $^{-1}$)	qe_{cal} (mg/ g)	qe_{exp} (mg/ g)	R^2
25	0.057	90.42	110.0	0.983	0.0016	115.84	110.0	0.991
40	0.023	93.32	90	0.823	0.0009	97.74	90	0.984
60	0.009	99.19	44	0.680	0.0017	48.79	44	0.977

3.3. Adsorption Kinetics and Mechanism of Iron

The data obtained from batch experiments which were performed at different temperatures (25–60) ^{0}C were evaluated by using the simple Lagergren equation to determine the adsorption rate of Iron interactions. The K_{lFe} values could be obtained by plotting log ($q_e - q_t$) versus t

for adsorption of Iron at different temperatures as shown in Figure (14). The values of the first order rate constant (K_{lFe}) and correlation coefficient (R^2) obtained from these plots are listed in Table 2. The values of K_{lFe} indicate that the rate of the process decreases with temperature.

The first order mechanism suffered from inadequacies when applied to iron sorption on the APNS. One of the major discrepancies was observed when q_e values obtained from the pseudo first order plots were compared with the experimental q_e values are seen in Table (5). The experimental q_e values differed from the corresponding theoretical values. Thus, the interaction of iron with the APNS does not follow the first order kinetics.

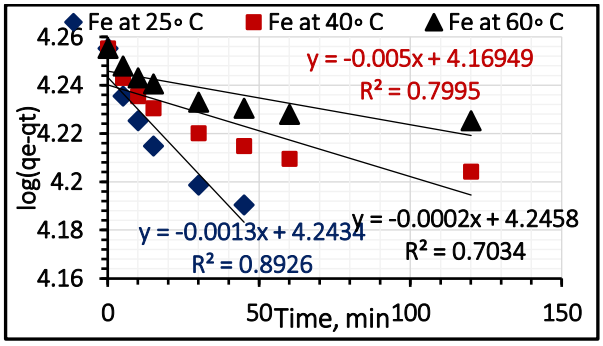

Fig (14): Pseudo second-order plots for the adsorption of iron

In order to insure the description of the kinetics, second order kinetic equation was applied. The kinetic plots of t/q_t versus t for uranium are shown in Figure (15). The plots show straight lines with good linearity temperatures. The calculated correlation coefficients are closer to unity for the pseudo second order kinetic model. The calculated equilibrium adsorption capacity (q_e) is consistent with the experimental data. The K_{2Fe} values show the applicability of the above equation for the resin. Therefore, the sorption reaction can be approximated more favorably by the pseudo second order sorption as the predominant mechanism.

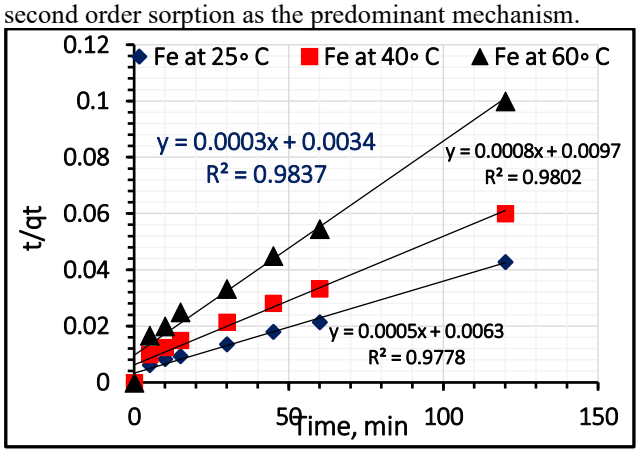

Fig (15): Pseudo second-order plots for the adsorption of iron

Table (5): Data of kinetic parameters for iron adsorption onto APNS

Temp, °C	Lagergreen pseudo first-order				pseudo second-order			
	K_1 (min^{-1})	q_{ecal} (mg/ g)	q_{eexp} (mg/ g)	R^2	K_2 (min^{-1})	qe_{cal} (mg/ g)	qe_{exp} (mg/ g)	R^2
25	0.0025	2800	1000	0.892	$3.1x10^{-5}$	2800	3062.07	0.983
40	0.0008	2000	1584.8	0.799	$3.3\ x10^{-5}$	2000	2188.39	0.977
60	0.0005	1200	2511.8	0.603	$5.9x10^{-5}$	1200	1314.19	0.980

3.4. Adsorption Isotherm of uranium

A number of common adsorption isotherm models were considered to fit the attained isotherm data under the equilibrium adsorption of the APNS. Examples of these models are Langmuir and Freundlich.

A- Langmuir Isotherm

Langmuir model suppose that, the adsorption occurs uniformly on the active sites of the sorbent, and once a sorbate occupies a site, no further sorption can take place at this site [48].

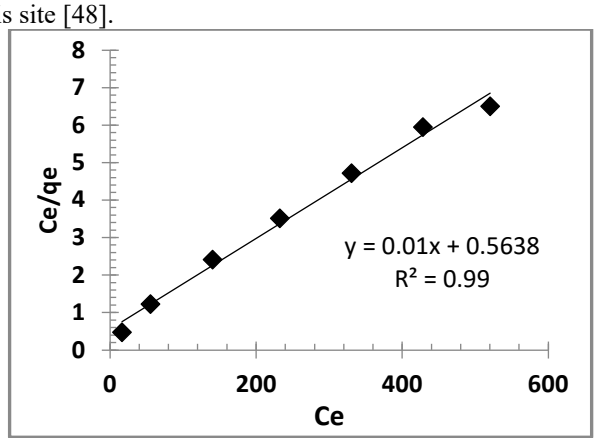

Fig (16): Langmuir isotherm plot for adsorption of uranium onto APNS

Thus, the Langmuir model is given by the following equation:

$$\frac{C_e}{q_e} = \frac{1}{bq_0} + \frac{C_e}{q_0} \qquad (7)$$

where: q_o and b, the Langmuir constants, are the saturated monolayer sorption capacity and the sorption equilibrium constant, respectively. A plot of C_e/q_e versus C_e would result in a straight line with a slope of $1/q_o$ and intercept of $1/bq_o$ as seen in Figure (16). The Langmuir parameters are given in Table (6).

B- Freundlich Isotherm

The Freundlich model stipulates that the ratio of solute adsorbed to the solute concentration is a function of the solution. The empirical model was shown to be consistent with exponential distribution of active centers, characteristic of heterogeneous surfaces [49].

The amount of solute adsorbed at equilibrium, q_e, is related to the concentration of solute in the solution, C_e, by the following:

$$q_e = K_F C_e^{1/n} \qquad (8)$$

This expression can be linearized to give:

$$\log q_e = \log K_F + \frac{1}{n}\log C_e \qquad (9)$$

where K_F and n are the Freundlich constants, which represent sorption capacity and sorption intensity, respectively. A plot of ($\log q_e$) versus ($\log C_e$) would result in a straight line with a slope of (1/n) and intercept of (log K_F) as seen in Figure (17). Freundlich constants are given in Table (7). Comparing the isotherms applied with the experimental results, Langmuir gave the best fit, while Freundlich isotherms did not fit well.

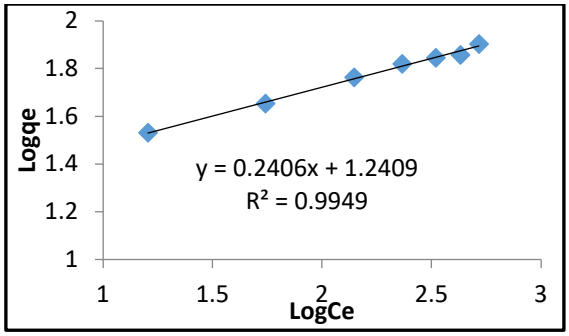

Fig (17): Freundlich isotherm plot for adsorption of uranium onto mesoporous carbon

Table (7): Langmuir and Freundlich isotherms parameters for uranium adsorption onto mesoporous carbon

Langmuir model parameters			Freundlich model parameters		
q_o (mg/g)	b (L/mg)	R^2	1/n	K_f (mg/g)	R^2
100.0	0.017	0.99	4.15	17.017	0.9949

3.5. Adsorption Isotherm of Iron

A- Langmuir Isotherm

According to Langmuir model, the adsorption occurs uniformly on the active sites of the sorbent, and once a sorbate occupies a site, no further sorption can take place at this site. A plot of C_e/q_e versus C_e would result in a straight line with a slope of $1/q_o$ and intercept of $1/bq_o$ as seen in Fig (18). The Langmuir parameters are given in Table (8).

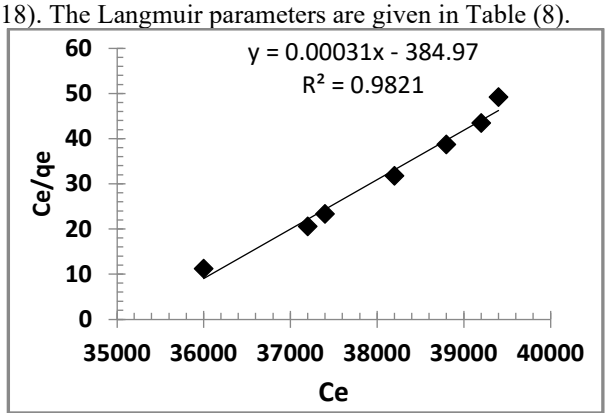

Fig (18): Langmuir isotherm plot for adsorption of Iron onto APNS

B- Freundlich Isotherm

The Freundlich model stipulates that the ratio of solute adsorbed to the solute concentration is a function of the solution. The empirical model was shown to be consistent with exponential distribution of active centers, characteristic of heterogeneous surfaces. A plot of ($\log q_e$) versus ($\log C_e$) would result in a straight line with a slope of (1/n) and intercept of (log K_F) as seen in Figure (19). Freundlich constants are given in Table (8). Comparing the isotherms applied with the experimental results, Langmuir gave the best fit, while Freundlich isotherms did not fit well.

Table (8): Langmuir and Freundlich isotherms parameters for Iron adsorption APNS

Langmuir model parameters			Freundlich model parameters		
q_o (mg/g)	b (L/mg)	R^2	1/n	K_f (mg/g)	R^2
3325.8	8.0 x10^{-7}	0.982	0.067	1584.8	0.990

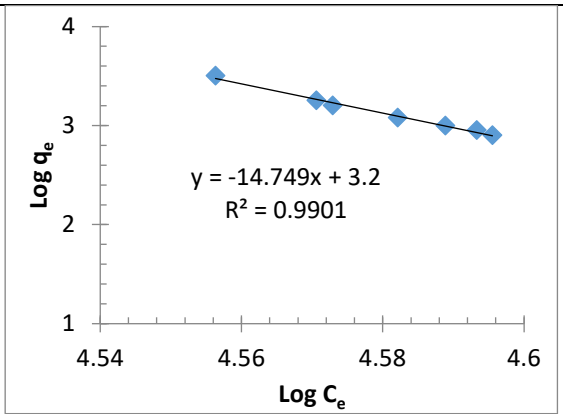

Fig (19): Freundlich isotherm plot for adsorption of iron onto APNS

3.6. Homogeneous diffusion model (HDM)

Homogeneous Particle Diffusion Model (HPDM) is the kinetic model which is widely used to describe the metal adsorption [50,51]. In this model, the extraction mechanism involves counter diffusion of metal ions from the aqueous solution and H^+ ions from the APNS phase through a number of possible resistances. The metal species originally in the solution phase must diffuse across the liquid film surrounding the APNS phase particle, transfer across the solution particle interface, diffuse into the bulk of the APNS phase particle and possibly interact with APNS reactive group. The species within the APNS reactive group simultaneously experience the same sequence in reverse order. The two main modes were film diffusion mode (FD) and matrix diffusion mode (MD) are given respectively, by Equations (10) and (11) which can be used to describe the rate of adsorption [52, 53]:

$$-\ln(1-X) = K_{FD}t \Rightarrow K_{FD} = \frac{3D_{FD}C_0}{rC_e\delta} \quad \ldots\ldots (10)$$

$$-\ln(1-X^2) = 2K_{MD}t \Rightarrow K_{MD} = \frac{\pi^2 D_{MD}}{r^2} \quad \ldots\ldots\ldots\ldots (11)$$

Where X is the fractional attainment of equilibrium ($X = q_t/q_e$) (assuming a constant value of the film thickness δ). The kinetic parameters for sorption of uranium and iron on APNS according to HPDM were estimated. The K_{FD} values for uranium and iron indicate that the diffusion coefficient in the liquid film (F_{MD}) were increases with the temperature. From the linear plot of function - ln (1-X) versus time t at different temperatures by using Eq. (10), as shown in figure (20), it is clear that the straight lines passing through the origin obtained for this relation is supported by a correlation coefficient (R^2) obtained around 0.80. Therefore, it is not satisfactory to explain the reaction by a film diffusion mode (FD) and the data did not fit at different temperatures.

On the other hand, the diffusion coefficients in matrix diffusion (DMD) can be estimated by using Eq. (11). The plots of function - ln ($1-X^2$) versus time t at different temperatures were shown in figure (21) for uranium and iron. The straight lines obtained passing thought the origin satisfactory represent the data based on the higher correlation coefficients (R^2) of 0.98.

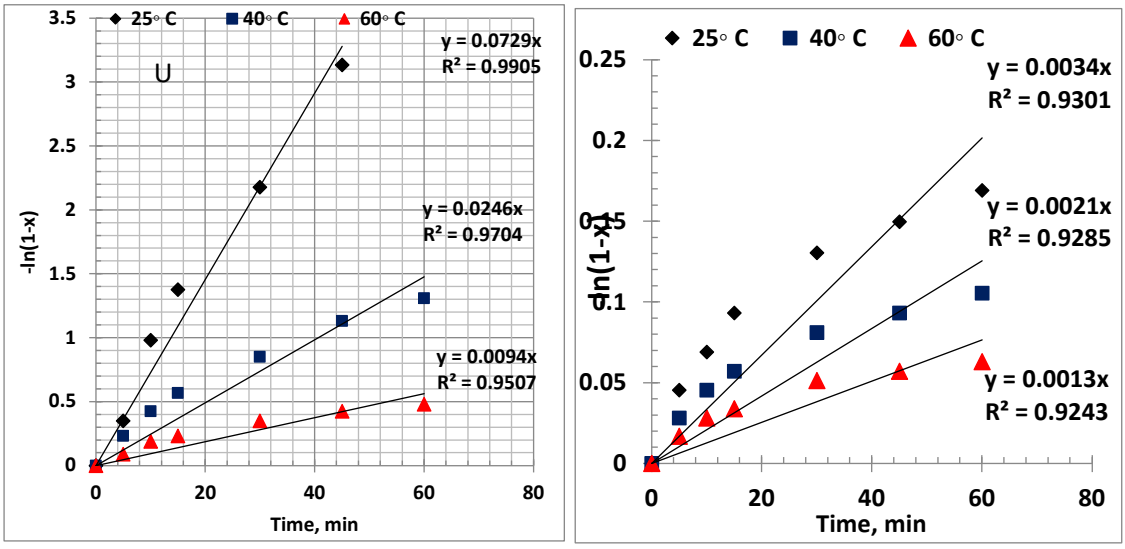

Fig (20): Film diffusion mode plots of uranium and iron sorption on APNS at different temperatures

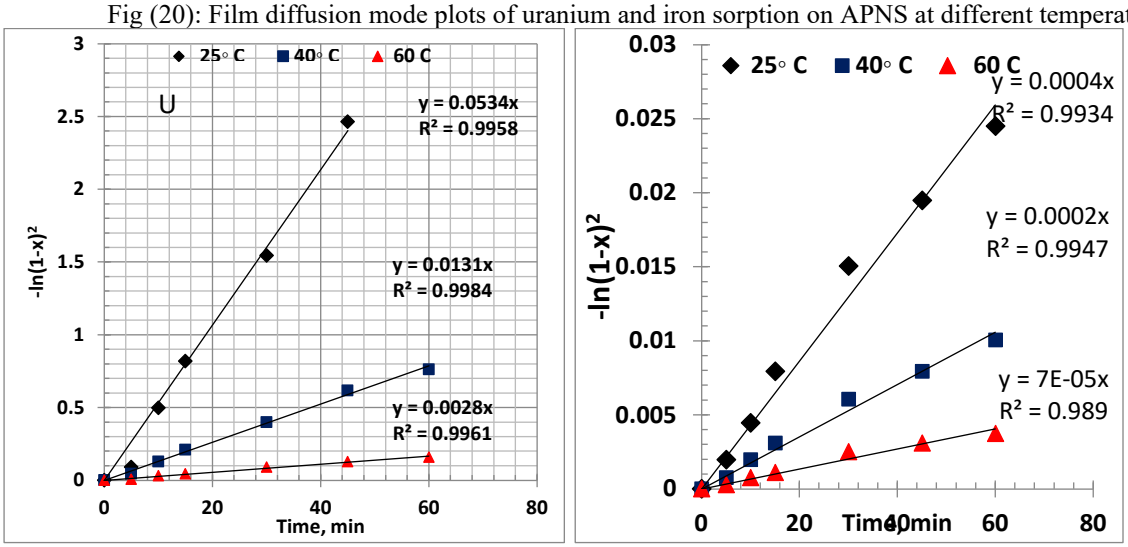

Fig (19): Matrix diffusion mode plots of uranium and iron sorption on APNS at different temperatures

3.7. Uranium desorption

Different desorbing reagents were used for the maximum desorption efficiency of U(VI). These include: 1 molar of Na_2SO_4, NaCl, HNO_3, H_2SO_4, and Na_2CO_3. The desorption experiments were carried out by stirring

4 g of loaded APNS with 15 ml eluent for 30 min. The results were summarized in Table (9), H_2SO_4 gives the best desorption efficiency of 90% for uranium a comping with 85% for iron.

Table (9): Effect of different types of eluents

Eluents, IM	Eluted U%	Eluted Fe%
Na_2SO_4	90	85
NaCL	80	78
HNO_3	56	70
H_2SO_4	90	88
Na_2CO_3	60	65

3.8. Case study

By stirring 0.01gm APNS with 15 ml of real sample of phosphoric acid contains 60 ppm uranium, 2.4% Fe, and P_2O_5 45% for 1 hour at room temperature. The results showed that, uranium and iron was removed by 66% and 36% respectively with only loss of P_2O_5 of 3%. Elution process carried out by stirring 15 ml H_2SO_4 with 4-gram loaded APNS for 30 min., the elution gave 78% U, 68% Fe, 3% P_2O_5.

3.9. Reusability of APSN

The regenerated adsorbent was used in repeated sorption desorption regeneration cycles up to eighteen cycles without significant decrease in sorption capacity.

4. Conclusion

Based on the results obtained from the study of the removal of uranium and iron from synthetic phosphoric acid by activated pistachio nutshell. the studied relevant factors of adsorption process have actually been optimized It was performed using one g AIC in 400 ml synthetic phosphate solution (35%) within 100 mg/L uranium at room temperature for 60 min. The capacity of uranium and iron were reached 54.5 mg/g and respectively. The elution of uranium and iron were performed using 30 ml of one mole Na_2CO_3 solution using 15 min contact time for each g of APNS. The isotherm studies show that the adsorption of uranium and iron could fit with Langmuir than Freundlish isotherm model. The adsorption reaction was suggested to follow pseudo-second-order model kinetics. APNS was used for removal of uranium and iron from areal sample of crude phosphoric acid supplied from phosphoric acid plant at nuclear materials authority. The results shown that removed of 12% and 55% for uranium and iron respectively with loss of P_2O_5 about 3%. APNS could be regenerated and reused for regeneration cycles up to eighteen cycles without significant decrease in sorption and breakthrough capacities. From results we can conclude that the APNS can be used in the removal of uranium and iron from crude phosphoric acid with highly efficiency.

References

[1] X. Li, J. Li, Y. Jin, M. Chen, D. Feng, Y. Guo, Wet process of phosphoric acid purification by solvent extraction using tri-n-butyl phosphate and cyclo hexanol mixtures. Journal of the Serbian Chemical Society. 82 (2017) 1-14.

[2] M. I. Amin, M.M. Ali, H.M. Kamal, A. M. Youssef, M.A. kl, Recovery of high-grade phosphoric acid from wet process acid by solvent extraction with aliphatic alcohols., Hydrometallurgy. 105(2010) 115-119.

[3] X. Jia, J. Li, Y. Jin, J. Luo, B. Wang, Y. Qi, Liquid−liquid equilibrium in the nitric acid/phosphoric acid/water/tri-n-octylamine system., Journal of Chemical & Engineering Data. 58 (2013) 78−83.

[4] M. Zeng, B. Liao, M. Lei, Y. Zhang, Q. Zeng, B. Ouyang, Arsenic removal from contaminated soil using phosphoric acid and phosphate, *Journal of Environmental Sciences* 20(1) (2008) 75-79.

[5] Uranium 2011: Resources, production and demand. A Joint Report by the OECD Nuclear Energy Agency and the International Atomic Energy Agency, IAEA, (2012).

[6] OECD (2016) Nuclear energy agency and international atomic energy agency. Uranium 2016: resources, production and demand. OECD.

[7] A. H. Orabi, E. M. El-Sheikh, W. H. Saleh, A. O. Youssef, M. Y. El-Kady, Z. M. Shalaby, Potentiality of uranium adsorption from wet phosphoric acid using amine-impregnated cellulose, a Journal of Radiation Research and Applied Sciences 9 (2016) 193 – 206.

[8] A.E.M. Hussein, A.M.A. Morsy, Uranium recovery from wet-process phosphoric acid by a commercial ceramic product, Arabian Journal of Chemistry (2017) 10, S361–S367.

[9] A. Ismail, Iron Removal from Phosphoric Acid by Precipitation Process, Central Metallurgical R&D Institute, Cairo, Egypt (1998).

[10] M. H. Abdallah, M. M. Kamel, Removal of Iron Ions from Phosphoric Acid Solution using Polyvinyl Alcohol and Zirconium Oxide Composite, Chemistry of Advanced Materials 3(2) (2018) 23-35.

[11] A.A. El-Asmy, Homam M. Serag, Mohammad A. Mahdy and Moustafa I. Amin; Purif. Tech., 61 (2008) 287.

[12] K. Schrödter, G. Bettermann, T. Staffel, T. Klein, T. Hofmann, Phosphoric Acid and Phosphates, in Ullmann's Encyclopedia of Industrial Chemistry. 2000, Wiley-VCH Verlag GmbH & Co. KGaA.

[13] Li, X., Li, J., Jin, Y., Chen, M., Feng, D., Guo, Y., Wet process of phosphoric acid purification by solvent extraction using tri-n-butyl phosphate and cyclohexanol mixtures, Journal of the Serbian Chemical Society. 82 (2017) 1-14.

[14] M. I. Amin, , M. M. Ali, , H. M. Kamal, , A. M. Youssef, M. A. Akl, , Recovery of high grade phosphoric acid from wet process acid by solvent extraction with aliphatic alcohols, Hydrometallurgy. 105 (2010) 115-119.

[15] S. Gogoi, S. K. Nath, S. Bordoloi, R. K. Dutta, Fluoride removal from groundwater by limestone

treatment in presence of phosphoric acid, Journal of Environmental Management 152 (2015) 132-139.
[16] M. Al-Harahsheh, Y. A. Hussain, H. Al-Zoubi, M. Batiha, E. Hammouri, Hybrid precipitation-nanofiltration treatment of effluent pond water from phosphoric acid industry, Desalination 406 (2017) 88-97.
[17] I. A. W. Tan, J. C. Chan, B. H. Hameed, L. L. P. Lim, Adsorption behavior of cadmium ions onto phosphoric acid-impregnated microwave-induced mesoporous activated carbon, Journal of Water Process Engineering 14 (2016) 60-70.
[18] L. Wu, W. Wan, Z. Shang, X. Gao, N. Kobayashi, G. Luo, Z. Li, Surface modification of phosphoric acid activated carbon by using non-thermal plasma for enhancement of Cu(II) adsorption from aqueous solutions, Separation and Purification Technology 197 (2018) 156-169.
[19] S. S. Metwally, I. M. Ahmed, H. E. Rizk, Modification of hydroxyapatite for removal of cesium and strontium ions from aqueous solution, Journal of Alloys and Compounds 709 (2017) 438-444.
[20] G. S. Sultanbayeva, R. Holze, R. M. Chernyakova, U. Z. Jussipbekov, Removal of Fe^{2+}, Cu^{2+}, Al^{3+} and Pb^{2+}ions from phosphoric acid by sorption on carbonate-modified natural zeolite and its mixture with bentonite, Microporous and Mesoporous Materials 170 (2013) 173-180.
[21] A. A. El-Zahhar, S. E. A. S. El-Deen, R. R. Sheha, Sorption of iron from phosphoric acid solution using polyacrylamide grafted activated carbon, Journal of Environmental Chemical Engineering 1(3) (2013) 290-299.
[22] R. Gani, C. Jiméner- Gonzàlez, A. Kate, P.A. Crafts, L. Powell, J.H. Atherton and J.L. Cordiner; J. Chem. Eng., 113 (2006) 30.
[23] A.A. El-Asmy, H. Serag, M. A. Mahdy and M. I. Amin; J. Separation and Purification Technology, 61 (2008) 287.
[24] H. Chen, Z. Sun, X. Song, J. Yu, Efficient Extraction of Phosphoric Acid with a Trialkyl Amine-Based Solvent Mixture, Journal of Chemical & Engineering Data. 61(2016) 438-443.
[25] Y. Ma, W. Zhou, J. Zhou, Effects of impurity ions on the metastable zone width of phosphoric acid in tributyl phosphate, Journal of Chemical & Engineering Data. 59 (2014) 2909-2913.
[26] C. Liu, Y. Ren, D. Tian, X. Zhang, Y. Wang, L. Kong, W. Shen, Equilibria of the quaternary system including phosphoric acid hydrochloric acid, water and tri-n-butyl phosphate at T = 303.2 K and atmosphere pressure, Journal of Chemical Thermodynamics. 79 (2014) 118-123.
[27] R. Sanghani, Novel Technique for Purification of Fertilizer Phosphoric acid with Simultaneous Uranium Extraction, *Procedia Engineering.* 83 (2014) 225-232.
[28] X. Jia, J. Li, Y. Jin, J. Luo, B. Wang, Y. Qi, Liquid−liquid equilibrium in the nitric acid/phosphoric acid/water/tri-n-octylamine system, Journal of Chemical & Engineering Data. 58 (2013) 78−83.
[29] Et. Ennaassia, K. El Kacemi, A. Kossir, G. Cote, Study of the removal of Cd(II) from phosphoric acid solutions by precipitation of CdS with Na2S, Hydrometallurgy. 64 (2002) 101-109.
[30] Y. A. El-Nadi, J. A. Daoud, , Sulphide precipitation of iron and its effect on the extraction of uranium from phosphoric acid medium, Journal of Nuclear and Radiochemical Sciences. 5 (2004) pp. 11-15.
[31] M. A. Abdulbaki, , Removal of fluoride from commercial Syrian wet phosphoric acid by precipitation, Indian Journal Chemical Technology. 14 (2007) 430-431.
[32] A. A. El-Bayaa, , N. A. Badawy, , A. M. Gamal, , I. H. Zidan, , A. R. Mowafy, , Purification of wet process phosphoric acid by decreasing iron and uranium using white silica sand, Journal of Hazardous Materials. 190 (2011) 324-329.
[33] M. H. SOLIMAN, H. S. GADO and M N. KOURAIM, Chemical Studies on the Removal of Iron from Crude Phosphoric Acid Using an Organosilicon Compound, E-Journal of Chemistry 2009, 6(S1), S329-S341.
[34] Adsorption of uranium from crude phosphoric acid using activated carbon Article *in* Journal of Radioanalytical and Nuclear Chemistry · May 2011 DOI: 10.1007/s10967-011-0980-7.
[35] A.A. El Zahhar, M. M. Ali, A. M. Ahmed, M. E. Khalifa, E. M. Abdel-Bary, Removal of iron from wet-process phosphoric acid using titanium silicate-polymercomposite, CTAIJ 10 (2015) 210-219.
[36] M. B. Chehid Elleuch, M. B.Amor, , G. Pourcelly, Phosphoric acid purification by a membrane process: electrodeionization on ion-exchange textiles, Separation and Purification Technology. 51 (2006) 285-290.
[37] M. P. Gonzalez, R. Navarro, I. Saucedo, M. Avila, J. Revilla, C. Bouchard, Purification of phosphoric acid solutions by reverse osmosis and nano filtration, Desalination. 147 (2002) 315-320.
[38] A.F. Tajar, T. Kaghazchi, M. Soleimani, Adsorption of cadmium from aqueous solutions on sulfurized activated carbon prepared from nut shells, 165 (2009) 1159–1164.
[39] J.C. Moreno-Piraján, L. Giraldo Activated carbon obtained by pyrolysis of potato peel for the removal of heavy metal copper (II) from aqueous solution, J. Anal. Appl. Pyrolysis., 90 (2011) 42-47.
[40] Q. Miao, Y. Tang, J. Xu, X. Liu, L. Xiao, Q. Che n, Activated carbon prepared from soybean straw for phenol adsorption, J. Taiwan Inst. Chem. Eng, 44 (2013) 458-465.
[41] H. Demiral, I. Demiral, Adsorption of chromium (VI) from aqueous solution by activated carbon derived from olive bagasse and applicability of different adsorption models, Chem. Eng. J., 15 (2008) 188-196.
[42] A. M. Al-Anber, Z.Al-Anber, Utilization of natural zeolite as ion exchange and sorbentmaterial in the removal of iron, Desalination, 255 (2008) 70-81.
[43] J.Z.Xiong, H.Q.Mahmood, D.Liu, Phosphate removal from solution using steel slag through magnetic separation, J.Hazard.Mater., 152 (2008) 21-1.215.

[44] A. Geethakarthi , R. Phanikumar, Adsorption of reactive dyes from aqueous solutions by tannery sludge developed activated carbon: kinetic and equilibrium studies, Int J Environ Sci Technol 8: (2011) 561–570 .
[45] J. Inglezakis, A. Stylianou, D. Gkantzou, D. Loizidou, Removal of Pb(II) from aqueous solutions by using clinoptilolite and bentonite as adsorbents, J Desalin 210 (2007) 248–256.
[46] S. Lagergren, Zur theorie der sogenannten adsorption gelo ¨ster stoffe Kungliga venska Vetenskapsakademiens. Handlingar 24(1898) 1–39.
[47] Y. S. Ho, and G. McKay, Pseudo-second order model for sorption processes, Process Biochem. 34 (1999) 451- 465.
[48] Langmuir, The adsorption of gases on plane surfaces of glass, mica and platinum, American Chemical Society, 40 (1918) 1361-1368.
[49] H. Freundlich, Adsorption in solution", Physical and Chemical Society, 40 (1906) 1361-1368.
[50] Y. M. Khawassek, A. A. Eliwa, E. A. Haggag, S.A. Omar and S.M. Abdel-Wahab, Adsorption of Rare Earth Elements by Strong Acid Cation Exchange Resin Thermodynamics, Characteristics and Kinetics SN applied Sciences, A SPRINGER NATURE journal, https://doi.org/10.1007/s42452-018-0051-6 (2019).
[51] H. Othman, M. Shabaan, M. Demerdash, andM. Saleh, Experimental and theoretical investigation of sorption kinetics of beryllium on Amberlite-IR-120 sorbent, J. of Nuclear Materials 392 (2009)427–433.
[52] S. G. Luque,, M. Streat, M., Uranium sorption from phosphoric acid solutions using selective ion exchange resins: Part I. Isotherms of extraction and desorption, Hydrometallurgy 11 (1983) 207-225.
[53] J. L. Cortina, N. Miralles, kinetic studies on heavy metal ions removal by impregnated resins containing di-(2,4,4-trymethylpentyl) phosphinic acid, Solv. Extr. Ion Exch. 15 (1997) 1067-1083.